Journal of Sound and Vibration (1994) **175**(4), 455–473

EFFICIENT OPTIMIZATION PROCEDURE FOR MINIMIZING VIBRATORY RESPONSE VIA REDESIGN OR MODIFICATION, PART II: EXAMPLES

I. BUCHER AND S. BRAUN

Technion—Israel Institute of Technology, Faculty of Mechanical Engineering, Haifa 32000, *Israel*

(*Received* 22 *April* 1992, *and in final form* 29 *March* 1993)

By using an optimization method presented in the companion paper, Part I, the optimal structural modifications leading to minimization of the vibratory response are found. A number of examples are given in this paper, from simple spring–mass systems to continuous finite element models of beams and plates. The application of the method for various cases provides illuminating results. As shown, one is able to attach engineering common sense to these solutions, in some cases, and to obtain insight about the nature of a dynamically optimal structure. Most results are interpreted by using frequency response functions, where the resulting modified structural resonance and anti-resonance frequencies, or the mode shapes, tend to behave in a special way related to the excitation and boundary conditions. The geometry of the optimized structure, as demonstrated in the paper, reflects the boundary conditions and force location. Some similarities between the optimized shape, resulting from a "dynamic" optimization, with shapes obtained by prior investigations dealing with only static deflections, can be noted. An experimental verification showing a simple case of point masses added to a vibrating beam shows good agreement of theory with the experimental results.

1. INTRODUCTION

Results of applying a method which allows the optimal selection of structural parameters, affecting the mass, stiffness and damping and hence the dynamic response, are presented and discussed. A suitable mathematical optimization was presented in the companion paper, Part I [1], in which the cost function is the vibratory response. Mathematical inequalities associated with the optimization problem impose constraints limiting the maximum allowed mass and bound the structure's geometrical dimensions within specified limits. This helps in defining a practical optimization with true engineering and design constraints. The excitation is defined by a shaping filter, driven by a random or an impulsive input. This allows one to specify a desired power spectral density (PSD) for the excitation. The following are the main features of the proposed method [1]. (i) Based on a defined response cost function, it was shown how to find an optimal solution for a range of excitations, both deterministic and random. (ii) A specific optimization problem definition, geared to vibratory systems, was formulated. (iii) A very efficient optimization process was developed, which is orders of magnitude faster than those based on traditional optimization approaches. (iv) The method developed can utilize either experimentally (incomplete) extracted information (modal testing) or analytically derived data (finite element methods).

0022–460X/94/340455 + 19 $8.00/0

The examples shown in this paper range from simple discrete spring–mass systems to finite element models of beams and plates. The optimization results are given for various excitation PSD, for a variety of boundary conditions and force locations. Given the results, the frequency response function and the mode shapes of the original and optimized structure are compared. Suitable interpretation is given where necessary.

The optimization of distributed parameter structures has been the subject of numerous references [2–4]. Most of the works deal with static deflections and stresses, with buckling loads and with the shift of natural frequencies. It can be noted that the general shapes obtained for optimized beams and plates are similar to some of the examples obtained in this work.

The paper is divided into case studies, the interpretation of the results supplying a physical understanding for each case. We show a number of examples demonstrating typical engineering problems which are amenable to our method. Appendices A, B and C explain various details concerning the optimization method. Appendix A describes the derivatives of the mass and stiffness matrices with respect to a change in a discrete spring or mass. Appendix B shows a similar development for a finite element model of a vibrating beam. Appendix C shows the realization of a narrow-band process used to describe the excitation used for some of the examples shown in the paper.

Example 1, which is of a tutorial character, is a discrete system. The fact that a solution, represented by one of many local minima for the vibratory amplitude, is not unique, is demonstrated. The physical meaning of each mathematical solution is explained. Example 2 demonstrates the application of the method when only a partial model is available (or, alternatively, when using a finite element model while considering a reduced number of extracted modes). Example 3 has a more practical flavor, showing how changes in the geometry of continuous elements can be used to minimize the response. A variety of optimized continuous beams with different boundary conditions, are discussed. These are subjected to narrow- and wide-band excitation. The nature of the optimized structure for each excitation is shown and explained. The optimized geometries have continuous shapes showing similarities to examples given in the literature [2–4] which consider buckling, shifting of natural frequencies, or static deflection and minimization of stresses. The shapes obtained agree with engineering intuition. Example 4 shows an application of the optimization method to a two-dimensional plate. Example 5 describes a simple experimental verification of the optimization method by applying an optimal set of discrete correction masses to a clamped beam. Formal definitions and the mathematical background are given in Part I [1].

2. EXAMPLE 1: A SIMPLE SPRING–MASS SYSTEM

The following examples describe the optimization of a series spring–mass system (see Figure 1). Two optimization runs are shown. For both cases, the initial structures have the same connectivity, as shown in Figure 1, but different values for the initial system parameters, m_i and k_i. The purpose of the comparison between the two systems is to explain the nature of a local minimum for the cost function by indicating its physical meaning.

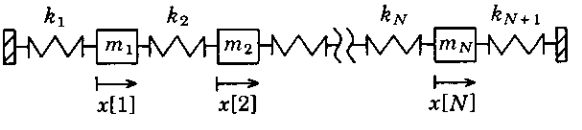

Figure 1. A series spring–mass system.

The structural parameters adjusted by the optimization scheme are the masses, $m_1, \ldots, m_N$ and the stiffnesses, $k_1, \ldots, k_{N+1}$. The derivatives of the mass and stiffness matrices with respect to the masses or springs are developed in Appendix B.

In order to demonstrate the method, we apply the outlined procedure for a four-degree-of-freedom (DOF) ($N = 4$) discrete structure. The optimization problem is defined mathematically as follows:

find $m_i, i = 1, \ldots, 4$; $k_i, i = 1, \ldots, 5$, such that the following conditions are met:

$$\text{cost function:} \quad J = \mathrm{E}[x[3]^2] \rightarrow \min.;$$

$$\text{constraint } g1: \quad 0{\cdot}7 \leqslant m_i \leqslant 70, \qquad 0{\cdot}7 \leqslant k_i \leqslant 70;$$

$$\text{constraint } g2: \quad \textit{total mass} = \sum_{j=1}^{4} m_j \leqslant 4. \tag{2.1}$$

Note that the problem (2.1) is identical to the cost function defined in Part I [1]. The excitation $f(t)$, which is of a narrow-band character, is described in Appendix C and is characterized by the central frequency $\omega_0 = 5$ and the bandwidth parameter $\zeta = 0{\cdot}001$. The excitation and response are at $x[3]$. The r.m.s. value of the excitation is taken as unity, as it does not have a special meaning here, since the system is assumed to be linear.

Two optimization runs, A and B, shown below, demonstrate the fact that the minimum obtained is a local one which depends on the initial system to be optimized (i.e., on the initial values of the design parameters vector). From the results obtained, the physical meaning of each local minimum can be understood, and thus the designer can take the appropriate steps to facilitate convergence to a selected (local) minimum.

2.1. EXAMPLE 1: PARAMETER SET A

The parameters are summarized in Table 1, and the frequency response function (FRF) amplitudes are shown in Figure 2.

TABLE 1

Initial and optimized values of masses and springs for case A

	m_1	m_2	m_3	m_4	k_1	k_2	k_3	k_4	k_5
Initial	0·7	0·907	0·7	1·693	20	20	20	20	9·7197
Optimized	0·7	0·7	0·7	1·9	70	20	70	41·972	3·613

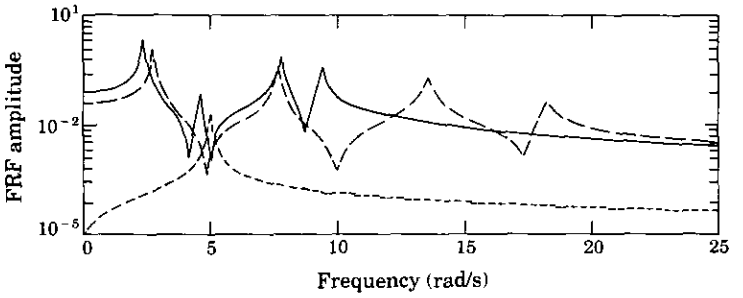

Figure 2. Frequency response function amplitudes for the original (——, r.m.s. value = 123) and optimized (– –, r.m.s. value = 23) structures for case A. - - -, FRF of excitation shaping system.

TABLE 2

Initial and optimized values of masses and springs for case B

	m_1	m_2	m_3	m_4	k_1	k_2	k_3	k_4	k_5
Initial	1	1	1	1	20	20	20	20	20
Optimized	0·7	0·7	0·7	0·7	70	70	70	70	70

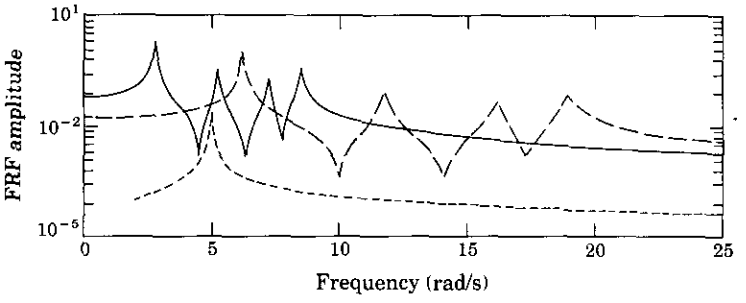

Figure 3. As Figure 2, but for case B, and optimized r.m.s. value = 99.

2.2. EXAMPLE 1: PARAMETER SET B

This example is defined as before but with one difference, the initial structure. The initial values for the masses and stiffnesses are chosen differently, as shown in Table 2. The FRF amplitudes are shown in Figure 3.

2.3. CONCLUSIONS FOR EXAMPLE 1, CASES A AND B

Case B demonstrates the "traditional" design approach. This approach tends to stiffen the structure in order to raise the first natural vibrating frequency above the excitation bandwidth. This result is obtained automatically when starting from the initial mass and stiffness given in Table 2. Other initial mass and stiffness values, as given for case A in Table 1, yield an anti-resonance (system zero in control terminology). As can be seen from Tables 1 and 2, the results for case A are much better (lower r.m.s. value at the specified point). It is important to stress that the optimization presented is with respect to a given excitation. Any uncertainty regarding the value of the excitation central frequency, ω_0, may be considered, by using an increased bandwidth (larger ζ). Other input characteristics may yield different frequency response functions (FRF's) for the optimum structure. For this case the two solutions obtained result from two different initial conditions, where each has a clear physical interpretation. The designer can perform an initial design step, where the natural frequencies are shifted. This will result in the convergence to a specific local minimum (a solution) having the specific properties such as anti-resonance or an increase in the lowest natural frequency.

3. RESPONSE OPTIMIZATION FOR A TRUNCATED MODEL

The following example is an application of the optimization procedure to a structure which is represented by a truncated modal model. This incompleteness of information requires a special procedure, which is represented by a specific constraint in the optimization problem. The optimization problem for experimentally obtained, truncated models is defined formally in Part I [1]. The actual, unmodified structure is shown in Figure 4, and the unmodified masses and stiffnesses are shown in Table 3.

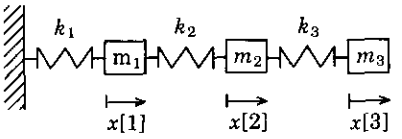

Figure 4. The three-mass discrete model.

TABLE 3

Unmodified model's masses and stiffnesses

m_1	m_2	m_3	k_1	k_2	k_3
1·5297	2·4644	1·941	250	250	250

3.1. OPTIMIZATION PROBLEM DESCRIPTION

We assume a truncated model including two (out of the three) modes. The numerical values of the right and left modal vectors and natural frequencies, Φ, L and Λ respectively, are

$$\Phi = \begin{pmatrix} 0{\cdot}2234 & 0{\cdot}4497 \\ 0{\cdot}4142 & 0{\cdot}3136 \\ 0{\cdot}5080 & -0{\cdot}4805 \end{pmatrix}, \qquad L = \begin{pmatrix} 0{\cdot}3417 & 0{\cdot}6879 \\ 1{\cdot}0208 & 0{\cdot}7730 \\ 0{\cdot}9860 & -0{\cdot}9327 \end{pmatrix}$$

$$\Lambda = \begin{pmatrix} \omega_1^2 & \\ & \omega_2^2 \end{pmatrix} = \begin{pmatrix} 23{\cdot}77 & \\ & 212{\cdot}87 \end{pmatrix}. \tag{3.1}$$

The permissible modifications, in this example, are discrete masses applied at the discrete degrees of freedom. Given the truncated model (two modes out of three) we wish to minimize the response to a narrow-band excitation with both at location $x[1]$. The excitation is a narrow-band one (see Appendix C for the definition) having a central frequency of $\omega_0 = 5$ and bandwidth parameter $\zeta = 0{\cdot}001$. The damping matrix, D, is assumed to behave according to $D = 0{\cdot}05M + 0{\cdot}001K$,

The formal definition of the optimization problem is as follows:

$$\min_{h} \mathrm{E}[x[1]^2]$$

$$\begin{aligned} \text{subject to} \quad & \text{constraint } g_1, \quad 0{\cdot}0001 < \Delta m_i < 6, \\ & \text{constraint } g_2, \quad \sum_{i=1}^{3} \Delta m_i \leqslant 6, \\ & \text{constraint } g_3, \quad \| (L\Gamma + \Delta M\tilde{X})\tilde{\Lambda} - (L\Lambda\Gamma + \Delta K\tilde{X}) \|_F = 0. \end{aligned} \tag{3.2}$$

Constraint g_1 forces physical realizability of the modifications. Constraint g_2 limits the amount of added mass (adding infinite mass is a trivial solution). Finally, constraint g_3 forces the first m (here $m = 2$) modes to be exactly from the span Φ. This constraint allows the use of a subset of the modal data and hence a truncated model, as described in detail in Part I [1].

3.2. EXAMPLE 2: RESULTS

The unmodified and modified (optimized) systems are described via FRF plots. The FRF amplitudes for the modified and unmodified models, respectively, are shown in

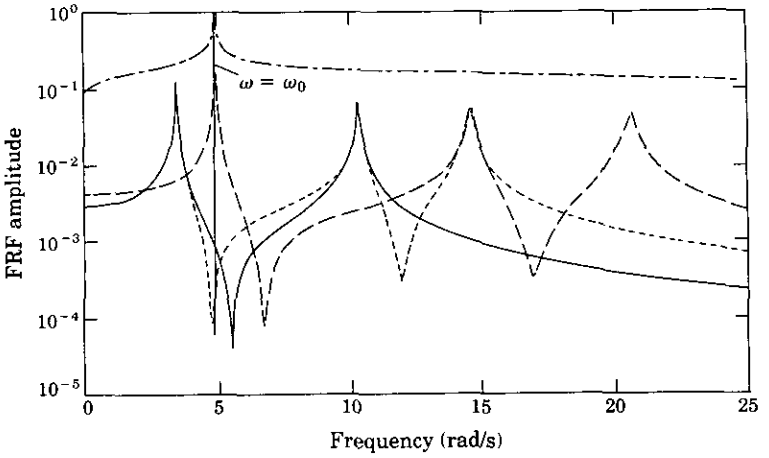

Figure 5. FRF amplitudes for modified (truncated), r.m.s. value = 9·1, structure (——), modified (full model), r.m.s. value = 8·5, structure (- - -), unmodified, r.m.s. value = 279, structure (—), and excitation shaping system (*not* to scale) (- - - -).

TABLE 4

Optimal amount of added mass at the three locations

Δm_1	Δm_2	Δm_3
1·546	2·49	1·96

Figure 5. Since the example is synthetic, we are able to compare the approximated optimization results for the truncated and the full models. Also shown in this plot is the FRF of the force shaping system.

The optimal amount of mass to be added at the three existing mass locations is tabulated in Table 4.

3.3. EXAMPLE 2: DISCUSSION AND CONCLUSIONS

Inspection of the FRF plots leads to the following conclusions and observations for these optimization results.

(a) The first two modified frequencies obtained for the full model match exactly (as this is the purpose of the constraint g_3) those represented by the truncated model. This observation comes from the fact that the corresponding resonance peaks of the full and truncated optimized models coincide.

(b) The reduction in the r.m.s. response in both the full and truncated models is very similar. This results from the fact that in the frequency region where the excitation is effective, the structure is represented fairly well by two out of the three modes.

(c) There is some difference in the location of the anti-resonance (the one in the vicinity of the excitation peak, $\omega = \omega_0$) between the full and truncated (optimized) models. Since the excitation in this example is a narrow-band one, the optimized yields, for the optimized model, an anti-resonance only in the vicinity of the excitation's peak. This inaccuracy is caused by the fact that the model is truncated.

(d) The condition forcing an exact assignment of natural frequencies, constraint g_3, prevents high amplitudes in the case of narrow-band excitation. This results from the fact that the optimization tries to drive the resonance frequencies away from the peak of the excitation. The sub-optimal optimization thus provides some robustness.

(e) We may encounter cases in which the narrow-band excitation may vary slightly, or not be known exactly. Also, anti-resonance points are shifted in the truncated model's case (as demonstrated here). The optimization can take advantage of the above-mentioned robustness and use a wider excitation bandwidth. This will result in a wider frequency region in which the structural amplification is low.

4. CONTINUOUS SYSTEM OPTIMIZATION: BEAMS

The following examples are of constant width beams having a variable profile (height). A beam having a varying profile is shown schematically in Figure 6. Also shown is the excitation acting at a specified location and the response, y, representing the response at specific locations where it is to be minimized. The vector of geometrical parameters, here composed of the beam's profile, is to be optimized with respect to given excitation and boundary conditions. The beam is modelled by a finite element (F.E.) model, with a constant height assumed within each element. The beam's F.E. model is described in Appendix B, as are also explicit expressions for the gradients with respect to the elements' height changes.

An optimization example for a clamped beam is formally defined here, and described in some detail in section 4.1. This is followed, in section 4.2, with a series of optimized beams for various excitations and boundary conditions.

The optimization problem is defined in a similar way for most of the examples in this section. The formal definition of the optimization problem is as follows:

$$\min_{h} \mathrm{E}[y^2]$$

$$\text{subject to constraint } g_1, \quad h_{min} \leqslant h_i \leqslant h_{max}, \quad i = 1, \ldots, NP,$$

$$\text{constraint } g_2, \quad \sum_{j=1}^{NP} h_j \leqslant (1+\epsilon) \sum_{j=1}^{NP} h_j^{initial} \quad (\epsilon \text{ maximum change in weight}). \tag{4.1}$$

4.1. CONTINUOUS BEAM OPTIMIZATION SUBJECT TO A BAND-LIMITED EXCITATION

The following example demonstrates the optimization of a cantilever beam, as modelled by six finite elements. The excitation generating function is similar to the one shown in example 1, but here the excitation bandwidth is much larger: i.e., $\omega_0 = 0{\cdot}25$ and $\zeta = 0{\cdot}2$. The formal definition of the optimization problem is given in equation 4.1. For this example $h_{min} = 0{\cdot}1$ and $h_{max} = 1$. The allowed increase in mass is 25%. The results are given, in a graphical description of the optimized beam, by FRF plots comparing the original FRF's to the optimized ones, and by the description of the spatial vibration amplitude resulting from a harmonic excitation.

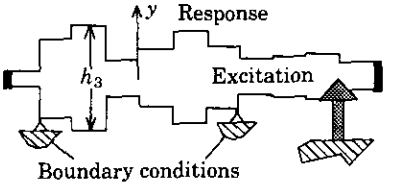

Figure 6. A beam with a varying profile.

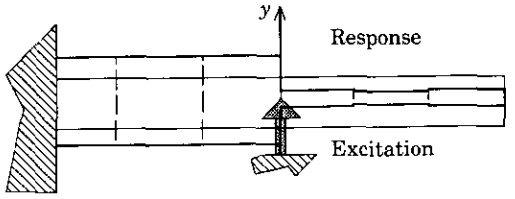

Figure 7. The beam's profile: ——, optimal beam; ——, original beam.

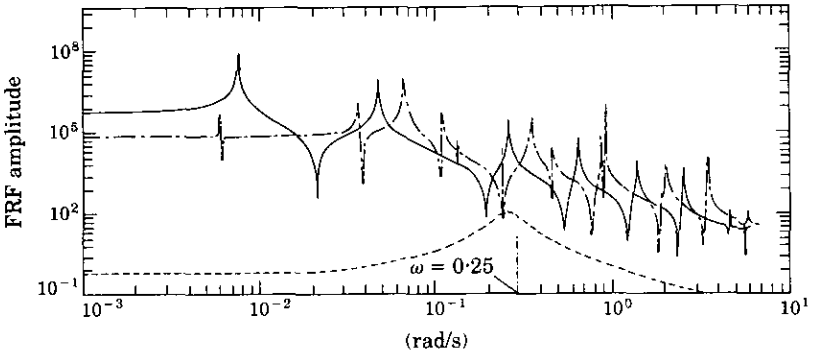

Figure 8. Amplitudes for the point FRF's of the original (——, r.m.s. value = 25·5) and optimized (– – –, r.m.s. value = 1·2) beams, and the excitation FRF (- - -).

The optimized beam's profile and the original profile, which is uniform, are shown in Figure 7. The optimized profile, represented by a thick line, is at its allowed maximum in the part between the clamp and the excitation.

The original and optimized amplitude FRF's are shown in Figure 8. These are compared to the force-shaping FRF, which is also plotted. The spatial vibration amplitudes for the unmodified and modified beams are shown in Figures 9(a) and (b).

In Figure 10 it is shown that the location, y, at which the response is minimized has a low vibration amplitude for a range of frequencies around the central one.

This example has demonstrated the use of a geometrical optimization for the minimization of response at specified locations. Inspection of Figure 7 shows that the r.m.s.

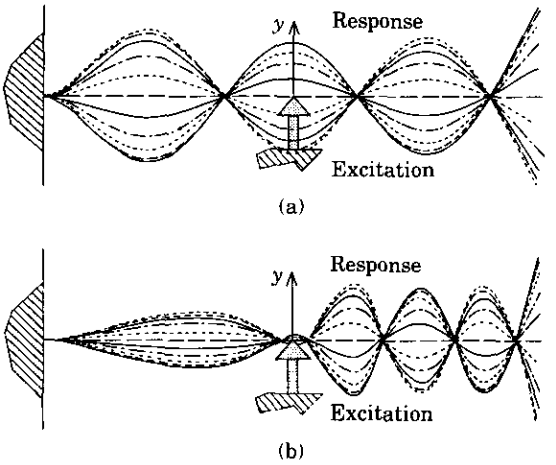

Figure 9. The spatial amplitude for harmonic vibration of $\omega = 0{\cdot}25$ Hz: (a) unmodified model; (b) optimized model.

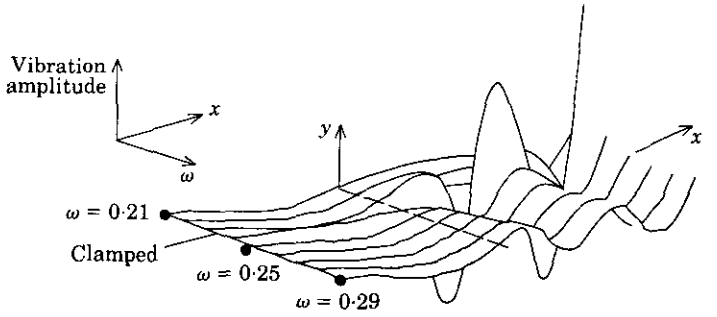

Figure 10. The vibration amplitude along the beam for harmonic excitations having different frequencies around the excitation peak.

response was decreased by a factor of 20. The point impedance at this point was increased, as can be seen from Figures 9(a) and (b). Close inspection of Figures 8 and 10 reveals that there is a resonance in the vicinity of the excitation peak. In our opinion this results from the fact that the excitation is not a narrow one (note the excitation width in Figure 8). Instead of pushing the resonance away from the frequency region in which the excitation has significant effect the optimization tried to eliminate its resonance behaviour by applying a nearby anti-resonance. This increased bandwidth excitation mimics a narrow-band excitation, with some uncertainty in the exact central frequency. Observation of Figure 10, which describes the vibration amplitude for various harmonic excitations with frequencies in the vicinity of the true excitation peak, shows that at the point at which vibrations are to be minimized a relatively low amplitude is preserved.

4.2. SHAPE OPTIMIZATION EXAMPLES: VARIOUS EXCITATION PSD'S AND BOUNDARY CONDITIONS

The outlined optimization procedure, given explicitly in equation (4.1) can be used to optimize the geometrical layout. As shown in Figures 11(a–f) different boundary

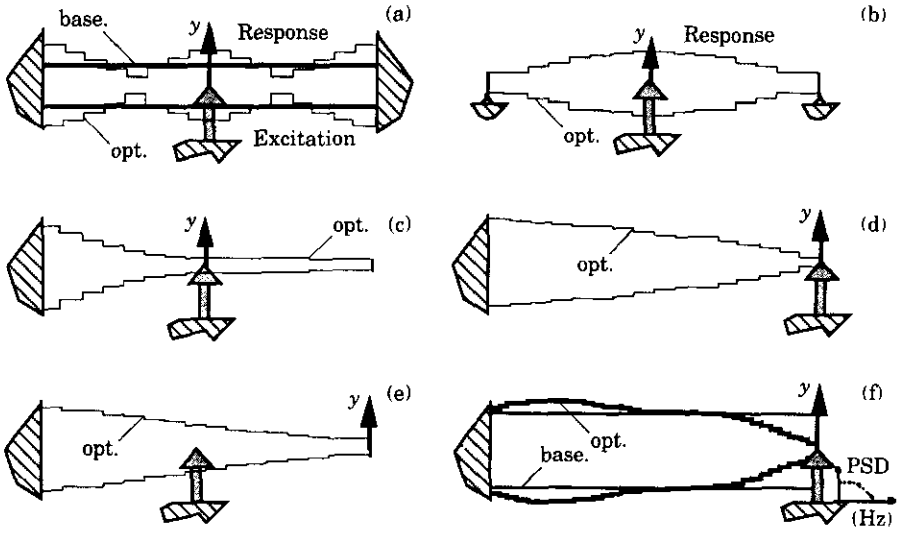

Figure 11. Optimized beams having various boundary conditions. (a) Baseline r.m.s. value = 22·1, optimized r.m.s. value = 1; (b) baseline r.m.s. value = 24·9 (uniform), optimized r.m.s. value = 2·17; (c) baseline r.m.s. value = 53·5 (uniform), optimized r.m.s. value = 2; (d) baseline r.m.s. value = 53·6 (uniform), optimized r.m.s. value = 2; (e) baseline r.m.s. value = 42 (uniform), optimized r.m.s. value = 2; (f) baseline r.m.s. value = 5, optimized r.m.s. value = 1.

conditions yield a few interesting shapes depicted here. The figures show the locations of the excitation and the sites at which the r.m.s. response is to be minimized. For examples (a–e) there is a narrow-band excitation and for example (f) a wide-band excitation.

The examples shown in Figures 11(a–e) are for a narrow-band excitation. It has been demonstrated by these that the geometrical layout of a structure can be designed to minimize the response at specific locations. In the case depicted in Figure 11(b), the initial design yields an increase in the first natural frequency above the excitation frequency, while in the case depicted in Figure 11(a) the optimization assigns an anti-resonance at a frequency close to the excitation's peak. The resulting shapes match, in general, those obtained for a related problem: maximization of the natural frequency with prescribed mass for the structure and minimization of the structural mass with prescribed natural frequency [2]. A similar shape is obtained for a maximization of a buckling load [3]. It is interesting to note that the shapes (profiles) obtained are continuous, although this was not a constraint in the optimization. The case shown in Figure 11(e), in which the excitation was applied at the middle of the beam and the response to be minimized was at the tip, it somewhat different. The FRF from the non-collocated force and measurement does not have the interlacing property of resonance and anti-resonance. Hence an assignment of an anti-resonance is not guaranteed. Nevertheless, in Figure 12(e), which demonstrates the results of the case in Figure 11(e), it is shown that the natural frequencies were shifted by the optimization to obtain an anti-resonance. The assignment of an anti-resonance resembles the application of a dynamic mass absorber [5] for a two-DOF system.

Case (f), for which the results are shown in Figure 13, demonstrates the application of the optimization method for a clamped beam exposed to an external force with flat characteristics in the excitation band. In this example, the optimization elmininates the resonance behavior in the range where the excitation is in effect. This is done by pole-zero cancellation or, in other words, by applying an anti-resonance near a resonance frequency.

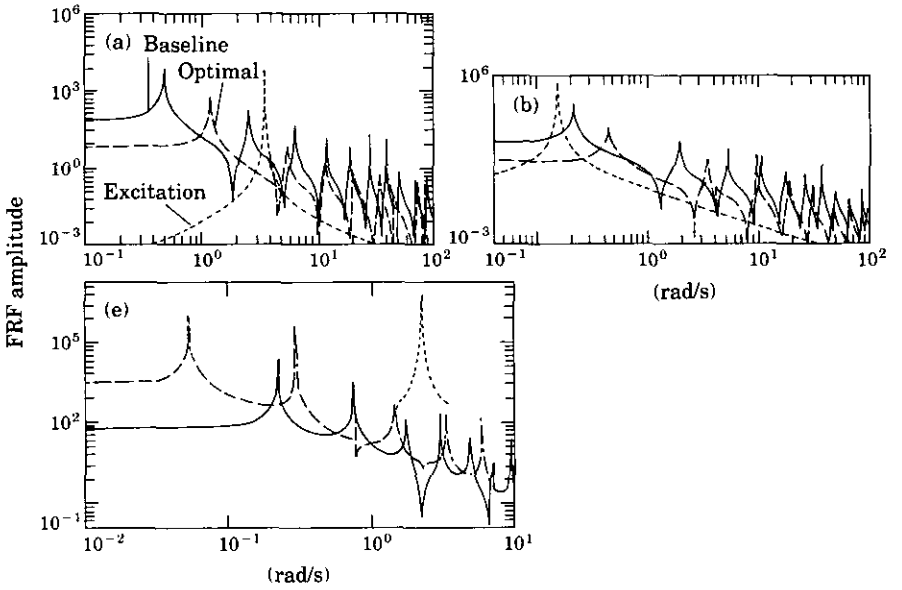

Figure 12. FRF responses for the baseline (——) and optimized (– –) beams of Figures 11(a), (b) and (e): - - -, excitation FRF.

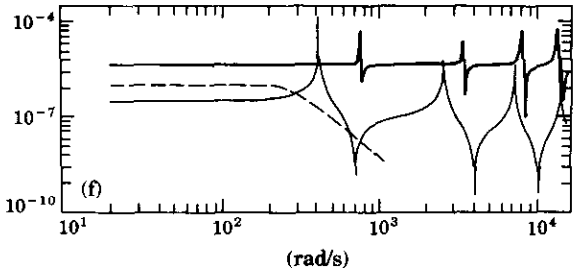

Figure 13. FRF responses for the baseline (——) and optimized (▬▬) beams of Figure 11(f), and for excitation (– –).

The constraints (see equation (4.1) for definitions) are an allowed 25% increase in total mass and an allowed minimum for the beam's height. It is interesting to note that the optimized beam did not have the maximum allowed mass. Another observation is related to the model used in the optimization process. As described in Part I [1], only some of the modes need be considered during the optimization process, as if the response were adequately represented by them. The plot in Figure 13 describes the FRF of the full model, i.e., containing all modes. It can be noticed that the optimization which considered only part of the modes gave an optimized beam with respect to the complete 36-elements F.E. model. This justifies the use of a truncated model for the optimization. A final remark concerns the static resistance of the structure: it can be seen that under a static load the structure is more flexible (this is concluded from the FRF near $\omega = 0$), although the converse is true for its dynamic behavior. This observation can be made by inspection of the FRF in the vicinity of $\omega = 0$ for both the original and optimized structures.

5. PLATE OPTIMIZATION

5.1. PLATE OPTIMIZATION: EXAMPLE 1

This example is an application of the optimization method to a vibrating plate. The plate is subjected to a point load characterized by a wide-band PSD. The purpose of the optimization is to minimize the vibration at the point at which the load is applied. The finite element mesh, the boundary conditions and the point at which the force is applied, are depicted in Figure 14. Also shown is the discretization of the plate into elements.

The optimization problem is defined mathematically in equation (4.1), but with the following structural constraints: (a) an allowed increase in mass of 25%; (b) a minimum

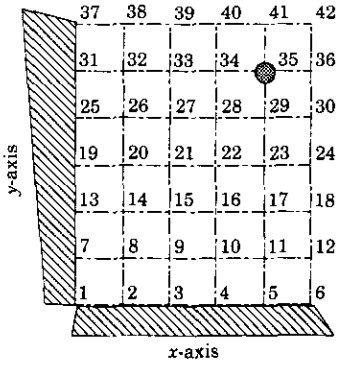

Figure 14. The plate F.E. Mesh.

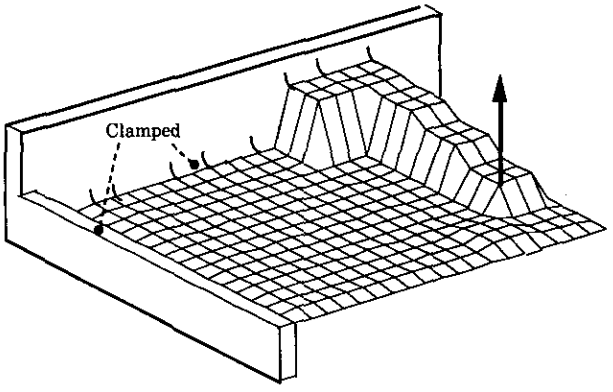

Figure 15. The optimized plate geometry.

thickness of 1·2 mm; and (c) a maximum thickness of 28 mm. The initial plate is uniform, having a thickness of 4 mm, and the plate dimensions are 680 × 670 mm.

The optimization results are as follows: initial cost function, $J(h_0) = 2{\cdot}99$; optimized structure's cost function, $J(h_{opt}) = 9{\cdot}6 \times 10^{-5}$; reduction in r.m.s. response, $\sqrt{J(h_0)/J(h_{opt})} = 177$.

The optimized plate is composed of a section similar to a cantilever beam, the optimized geometry yields a connection to the nearest clamping location as can be seen in Figure 15. This agrees with engineering intuition. The FRF plot in Figure 16 shows the elimination of the resonance behavior in the frequency region in which the force is in effect. This cancellation was also observed in Figure 13 for a clamped beam. The reduction in vibration is quite large compared to the mass added. This is expected since the original lay out was far from optimal.

5.2. PLATE OPTIMIZATION: EXAMPLE 2

This example is of an optimized clamped plate (four sides). The results show a large reduction in the vibratory response, and it can be concluded that this is a generalization of the clamped beam case in terms of the profile obtained. For convenience, we allowed a large amount of mass addition (ten times the original mass).

The finite element mesh is an 18 × 18 grid (total of 324 elements). The plate has two axes of symmetry. Hence, for the case where an excitation is applied at the mid-plate and

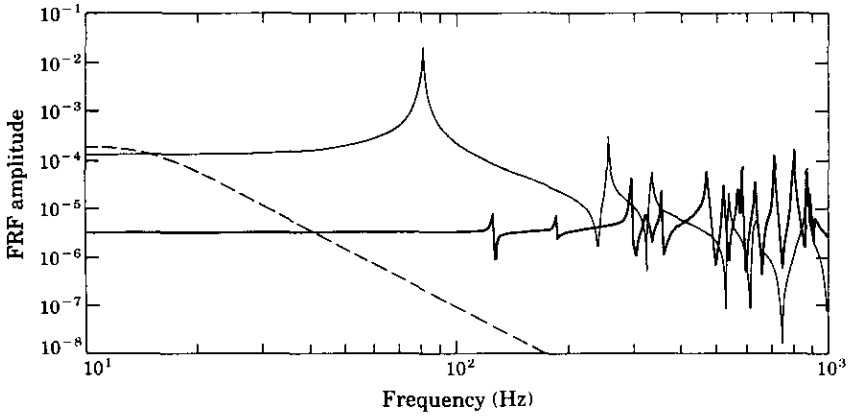

Figure 16. FRF's of the original (——) and optimized (▬▬) plates, and of the excitation (–·–).

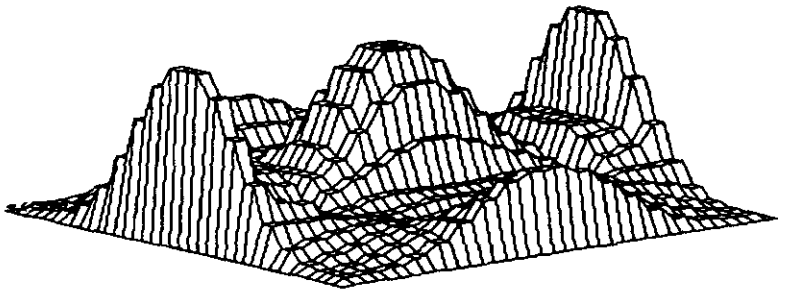

Figure 17. The optimized plate profile.

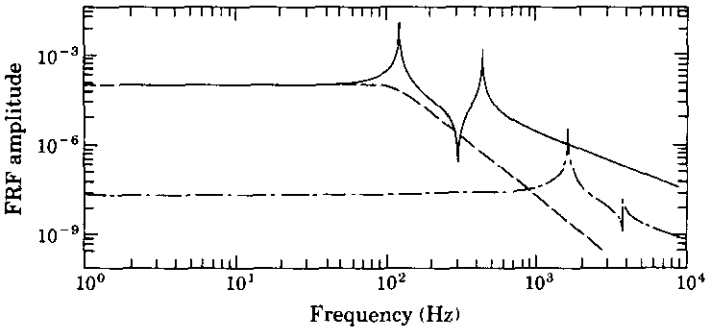

Figure 18. FRF amplitudes for the original (r.m.s. value = 0·32, ——) and optimized (r.m.s. value = 0·000016, – –) plates, and the shaping filter excitation (– · –).

the response is measured at the same location, all antisymmetric modes can be disregarded. Consequently, a quarter-plate model (9 × 9 with a total of 81 elements) is adequate.

The cost function is, as before, measure for the r.m.s. response at a specific point, while the constraints limit the amount of added mass. The optimized profie is depicted in Figure 17.

The r.m.s. response at each degree of freedom can be calculated by solving the appropriate Lyapunov equation, as described in Part I [1]. This can be used to describe an r.m.s. deflection resulting from the applied excitation, as shown in Figure 18. The r.m.s. deflections of the original and optimized plates differ very much in this case, since a large increase (ten times) in mass was allowed here (for the sake of fast convergence). A similar shape is obtained, but having different proportions, for the case in which a lesser amount of mass addition is allowed. The deflection amplitude for this case is depicted in Figure 19.

The character of the vibratory amplitude for the optimized plate is depicted in a magnified form in Figure 20.

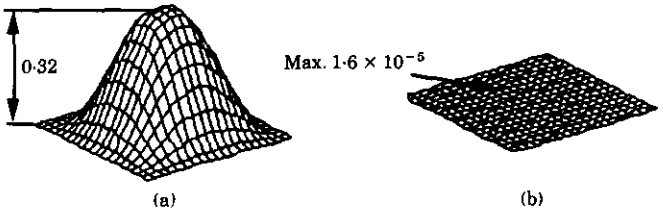

Figure 19. R.m.s. deflection shapes of the (a) original and (b) optimized plates.

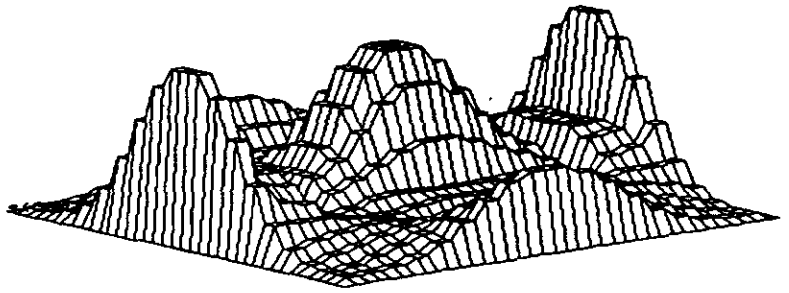

Figure 17. The optimized plate profile.

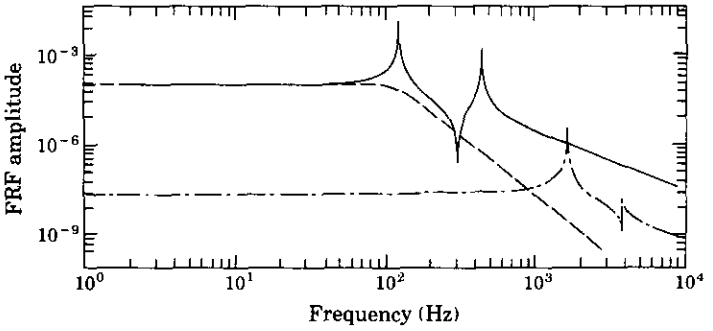

Figure 18. FRF amplitudes for the original (r.m.s. value = 0·32, ——) and optimized (r.m.s. value = 0·000016, – –) plates, and the shaping filter excitation (– · –).

the response is measured at the same location, all antisymmetric modes can be disregarded. Consequently, a quarter-plate model (9 × 9 with a total of 81 elements) is adequate.

The cost function is, as before, measure for the r.m.s. response at a specific point, while the constraints limit the amount of added mass. The optimized profie is depicted in Figure 17.

The r.m.s. response at each degree of freedom can be calculated by solving the appropriate Lyapunov equation, as described in Part I [1]. This can be used to describe an r.m.s. deflection resulting from the applied excitation, as shown in Figure 18. The r.m.s. deflections of the original and optimized plates differ very much in this case, since a large increase (ten times) in mass was allowed here (for the sake of fast convergence). A similar shape is obtained, but having different proportions, for the case in which a lesser amount of mass addition is allowed. The deflection amplitude for this case is depicted in Figure 19.

The character of the vibratory amplitude for the optimized plate is depicted in a magnified form in Figure 20.

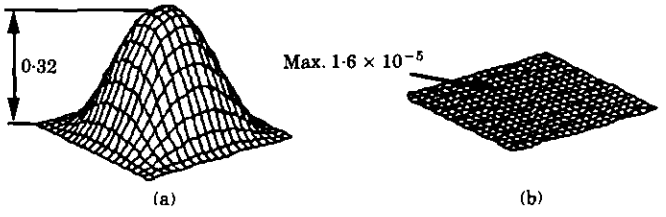

Figure 19. R.m.s. deflection shapes of the (a) original and (b) optimized plates.

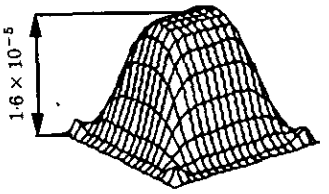

Figure 20. The magnified r.m.s. deflection shape of the optimized plate.

The effect of the optimization can also be visualized by comparing the original and optimized beams' frequency response functions (FRF's). The FRF's represent the responses at the middle of the plate to an excitation applied at the same point. The excitation is characterized by white noise filtered by a shaping filter, the FRF of which is given in the same figure.

This example is a generalization of the clamped beam optimization shown in Figure 11(a). Inspection of Figure 17 reveals that the profile in two perpendicular axes has a shape similar to that depicted in Figure 10(a). The boundary conditions here allow a large reduction of the vibratory amplitude as these provide considerable support to the plate. It can be observed that the resulting geometry is of a continuous nature, although this is not a specific constraint in the optimization's problem definition. The similarity of the geometry obtained to that for the buckling problems given in reference [4] should also be mentioned.

6. EXPERIMENTAL VERIFICATION: CLAMPED BEAM

The following example is an application of the optimization procedure described in Part I [1] to a real structure. A clamped beam, excited at the free end by a narrow-band excitation, is to be optimized by applying discrete masses at preselected locations. The optimization task is to find the optimal amount of mass to be applied at each location so as to minimize the vibration at the excitation point. The beam is described by a 13-element F.E. model and a similar discretization is performed physically on the real structure. The clamped beam and the mechanical arrangement for the masses to be added are shown in Figure 21.

The optimization seeks to minimize the vibration at the beam's tip by adding discrete masses at 13 locations. The optimization problem is defined as follows:

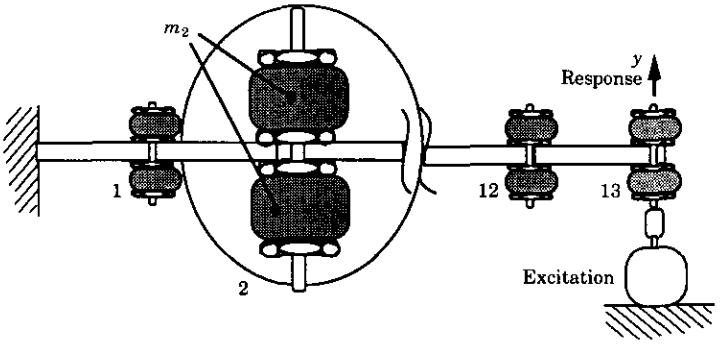

Figure 21. The clamped beam and the discrete masses to be added. Dimensions: length $L = 680$ mm; cross-section $b \times h$, with $b = 18{\cdot}85$ mm and $h = 5{\cdot}5$ mm.

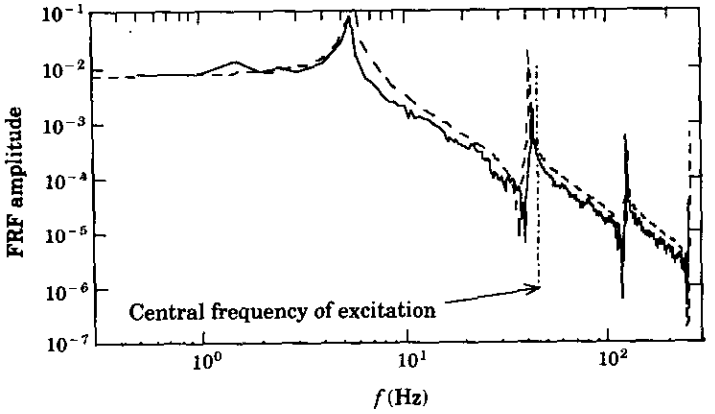

Figure 22. FRF amplitudes of the unmodified structure: - - -, analytic (F.E.); ——, measured.

$$\text{cost function,} \quad J = \mathrm{E}[y^2] \rightarrow \min.;$$

$$\text{constraint } g_1, \quad 0 \leqslant m_i \leqslant 0{\cdot}55 \text{ kg};$$

$$\text{constraint } g_2, \quad \textit{total mass} = \sum_{j=1}^{13} m_j \leqslant 0{\cdot}936 \text{ kg}. \tag{6.1}$$

A good agreement between the results from the finite element model and from the real structure was observed. This is evident from Figure 22, which shows two frequency response functions: an analytical one (F.E. based) and an FRF measured one for impulsive excitation, by means of an acceleration sensor and a commercial structural analyzer.

The optimal masses resulting from the optimization program were applied both to the finite element model of the structure and to the real structure. The resulting FRF plots

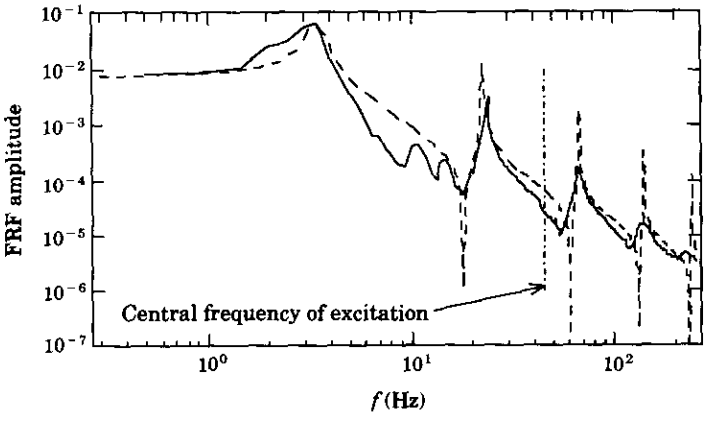

Figure 23. As Figure 22, but for the modified structure.

TABLE 5

Optimization results: optimal discrete masses to be added (kg)

m_1	m_2	m_3	m_4	m_5	m_6	m_7	m_8	m_9	m_{10}	m_{11}	m_{12}	m_{13}
0	0	0	0	0	0·096	0·12	0·12	0·12	0·12	0·12	0·12	0·12

are compared in Figure 23, and the optimal discrete masses to be added are shown in Table 5.

The results can be summarized as follows. The optimization procedure has been applied to a simple structure. By using a simple modification consisting of added discrete masses, the resonance frequency causing a large response was shifted. The optimization resulted in a considerable reduction in the amplification of the excitation by assigning an anti-resonance at the frequency at which the excitation is a maximum. The computer model and experimental results agree very well. For this particular selection of excitation frequency, the r.m.s. response has been reduced by a factor of 50.

6. CONCLUSIONS

This paper has dealt with the optimization of structural parameters, subject to constraints, in order to minimize the vibratory response. The theory was presented in Part I [1], and the present paper has provided specific examples.

The examples covered a wide range of problems, including very simple discrete systems as well as continuous one- and two-dimensional elements.

The examples also have included a case in which only a partial modal set was available, as a baseline model. In this case, special attention was paid to the interpretation of the optimized structural response. The deviation from optimality caused by the truncation of the model was investigated. In all cases, our method has converged to an optimized set of structural parameters which agree with "engineering common sense", and which reduce the vibratory response considerably. We thus believe that the approach described is well suited to handle actual engineering problems for structures. The relevant optimization runs for the described models were solved by using a microcomputer (386-PC), with solution times typically taking minutes. We thus conclude that it can be practically implemented into existing software packages (finite element and modal analysis) and serve as a valuable engineering design-aid tool.

REFERENCES

1. I. BUCHER and S. G. BRAUN 1994 *Journal of Sound and Vibration* **175,** 433–453. Efficient optimization procedure for minimizing vibratory response, part I: theory.
2. R. T. HAFTKA Z. GURDARD and M. P. KAMAT 1990 *Elements of Structural Optimization.* Dordrecht, The Netherlands: Kluwer.
3. C. A. BREBBIA and S. HERNANDEZ 1989 *Computer Aided Optimum Design of Structures: Recent Advances.* Berlin: Springer-Verlag.
4. E. J. HAUG and J. CEA 1981 *Optimizaiton of Distributed Structures, Volume I.* Alphen van den Rijn: Sijthoff and Noordhoff.
5. J. P. DEN HARTOG 1956 *Mechanical Vibration.* New York: McGraw-Hill.
6. G. M. L. GLADWELL 1986 *Inverse Problems in Vibrations.* The Hague: Martinus Nijhoff.

APPENDIX A: DISCRETE, SERIES SPRING–MASS MODEL—DERIVATION OF GRADIENT EXPRESSIONS

The system shown in Figure 1, for which the formulation is presented here, has a particular compact form, and hence, is suitable for illustrative purposes. The mass and stiffness matrices can be expressed as [5]

$$M = \operatorname{diag}_r \{m_r\}, \qquad K = E \operatorname{diag}_r \{k_r\} E^{\mathrm{T}} + k_{n+1} e_n e_n^{\mathrm{T}}, \tag{A1}$$

where

$$E = \begin{bmatrix} 1 & -1 & 0 & 0 \\ 0 & 1 & -1 & 0 \\ \vdots & 0 & 1 & -1 \\ 0 & 0 & 0 & 1 \end{bmatrix}$$

and e_n is the nth column of I_n.

The derivatives of the mass and stiffness matrices with respect to the mass and stiffness changes (required for the optimization process) can be expressed as

$$\mathrm{d}M/\mathrm{d}m_i = e_i e_i^{\mathrm{T}}, \quad \mathrm{d}K/\mathrm{d}k_i = E e_i e_i^{\mathrm{T}} E^{\mathrm{T}}, \quad 1 \leqslant i \leqslant n, \qquad \mathrm{d}K/\mathrm{d}k_{n+1} = e_n e_n^{\mathrm{T}}. \tag{A2}$$

Using a state space formulation (equations (4) of part I) for the vibrating system and the matrix identity

$$\mathrm{d}M^{-1}/\mathrm{d}m_i = -M^{-1}(\mathrm{d}M/\mathrm{d}m_i)M^{-1}, \tag{A3}$$

one is able to express the matrix derivatives under the assumption that the damping matrix, D, is small, and is not affected by point-wise modifications. We actually assume that the optimization process is intended to redistribute the energy in the structure rather than to dissipate it. Using equations (A2) and (A3) one obtains

$$\frac{\mathrm{d}}{\mathrm{d}m_i} A = \begin{bmatrix} 0 & 0 \\ \dfrac{1}{m_i^2} e_i e_i^{\mathrm{T}} K & \dfrac{1}{m_i^2} e_i e_i^{\mathrm{T}} D - M^{-1} \dfrac{\mathrm{d}D}{\mathrm{d}m_i} \end{bmatrix},$$

$$\frac{\mathrm{d}}{\mathrm{d}k_i} A = \begin{bmatrix} 0 & 0 \\ -M^{-1} \dfrac{\mathrm{d}K}{\mathrm{d}k_i} & 0 \end{bmatrix}, \qquad \frac{\mathrm{d}}{\mathrm{d}m_i} B = \begin{bmatrix} 0 \\ -\dfrac{1}{m_i^2} e_i e_i^{\mathrm{T}} \end{bmatrix}, \tag{A4}$$

where the usual assumption of proportional damping (i.e., $D = \alpha M + \beta K$), yields $\mathrm{d}D/\mathrm{d}m_i = \alpha\, \mathrm{d}M/\mathrm{d}m_i$.

These formulae are closed form expressions for the matrix derivatives with respect to mass and stiffness changes.

APPENDIX B: BEAM FINITE ELEMENT MODEL—DERIVATION OF GRADIENTS

The mass and stiffness matrices for a Bernoulli–Euler beam when using a F.E. formulation can be expressed as

$$M = \sum_{e=1}^{NE} M_e^{element}, \qquad K = \sum_{e=1}^{NE} K_e^{element}, \tag{B1}$$

where $M_e^{element}$ and $K_e^{element}$ are the element mass and stiffness matrices $m_e^{element}$ and $k_e^{element}$, extended (by adding zeros) to the size of the global matrices. The co-ordinate system shown in Figure B1 is used for each element. Using the definition of element co-ordinates in Figure B1, one can write the element matrices as

$$k_e^{element} = (Eb_e/12l_e^3)h_e^3 k_0, \qquad m_e^{element} = (\rho b_e l_e/420)h_e m_0,$$

$$k_0 = \begin{bmatrix} 12 & 6 & -12 & 6 \\ 6 & 4 & -6 & 2 \\ -12 & -6 & 12 & -6 \\ 6 & 2 & -6 & 4 \end{bmatrix}, \qquad m_0 = \begin{bmatrix} 156 & 22 & 54 & -13 \\ 22 & 4 & 13 & -3 \\ 54 & 13 & 156 & -22 \\ -13 & -3 & -22 & 4 \end{bmatrix}. \tag{B2}$$

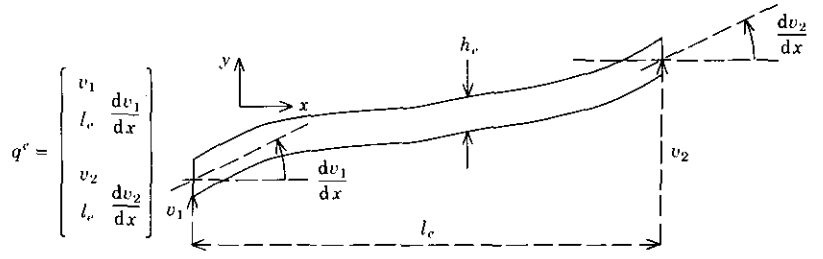

Figure B1. The constant height beam element and the generalised coordinates.

The derivatives of the mass and stiffness matrices with respect to a geometrical parameter are easily obtained by differentiation of equations (B1) with respect to the appropriate parameter:

$$\frac{dM}{dh_i} = \sum_{e=1}^{NE} \frac{dM_e^{element}}{dh_i} = \frac{dM_i^{element}}{dh_i}, \qquad \frac{dK}{dh_i} = \sum_{e=1}^{NE} \frac{dK_e^{element}}{dh_i} = \frac{dK_i^{element}}{dh_i} \tag{B3}$$

In this particular example, we obtain the required matrices by expanding the element gradient matrices to the global matrix size. The explicit expressions for a constant height element are

$$dk_e^{element}/dh_e = (Eb_e/4l_e^3)h_e^2 k_0, \qquad dm_e^{element}/dh_e = (\rho b_e l_e/420)m_0. \tag{B4}$$

Note that the derivative of the element mass matrix with respect to height is constant. Hence, this need be calculated only once during the optimization process.

Using the state space formulation (B4), one is able to express the derivatives of the matrices as

$$\frac{dA}{dh_i} = \begin{bmatrix} 0 & 0 \\ -\left(\Theta_i K + M^{-1}\frac{dK}{dh_i}\right) & -\Theta_i D - M^{-1}\frac{dD}{dh_i} \end{bmatrix}, \qquad \frac{dB}{dh_i} = \begin{bmatrix} 0 \\ \Theta_i \end{bmatrix}, \tag{B5}$$

where $\Theta_i = -M^{-1}(dM/dh_i)M^{-1}$ and $dD/dh_i = \alpha\, dM/dh_i + \beta\, dK/dh_i$.

These formulae are closed form expressions for the matrix derivatives with respect to a geometrical parameter. When using finite element methods for assembling the global mass and stiffness matrices from pre-defined element matrices, the expressions for the derivatives of element matrices with respect to a structural parameter can be stored in a library of elements. Such a library for the gradient matrices can be assembled similarly (or even by using the same code) from element based matrices.

APPENDIX C: NARROW-BAND EXCITATION—DESCRIPTION IN STATE SPACE

A narrow-band excitation, used in most of the examples here, can be described by using the state space realization

$$\dot{q}(t) = A_f q(t) + B_f e(t), \qquad f(t) = C_f q(t), \tag{C1}$$

where

$$A_f = \begin{bmatrix} -\zeta\omega_0 & -\omega_0 \\ \omega_0 & -\zeta\omega_0 \end{bmatrix}, \qquad B_f = \begin{bmatrix} 0 \\ 1 \end{bmatrix}, \qquad C_f = [1 \quad 0].$$

A typical value for ζ, used in this paper, is 10^{-3}. A representative PSD is shown in Figure C1.

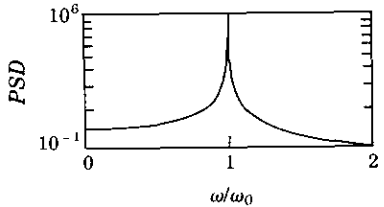

Figure C1. The PSD of a narrow-band function realized by equation (C1).

For a white noise excitation, $e(t)$, having the variance $\mathrm{cov}[e] = \sigma_e^2$, the PSD of the generated force would be

$$S_{ff}(\omega) = \frac{\sigma_e^2}{\omega_0^2(1 - 2(\omega/\omega_0) + (\omega/\omega_0)^2 + \zeta^2)(1 + 2(\omega/\omega_0) + (\omega/\omega_0)^2 + \zeta^2)}. \qquad \text{(C2)}$$